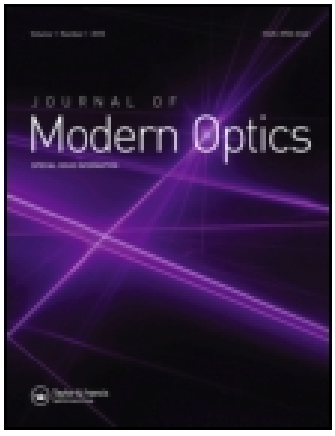

Journal of Modern Optics
Publication details, including instructions for authors and subscription information:
http://www.tandfonline.com/loi/tmop20

# Resonant nonlinearity enhancement in rubidium vapor with additional optical pumping

N. Korneev[a], Y.M. Torres[a], C. Gutiérrez-Parra[a] & Y. Ortega[a]
[a] Instituto Nacional de Astrofísica, Óptica y Electrónica, Puebla, México
Published online: 14 May 2014.

*Journal of Modern Optics*, 2014
Vol. 61, No. 12, 1009–1017, http://dx.doi.org/10.1080/09500340.2014.917730



# Resonant nonlinearity enhancement in rubidium vapor with additional optical pumping

N. Korneev, Y.M. Torres*, C. Gutiérrez-Parra and Y. Ortega

*Instituto Nacional de Astrofísica, Óptica y Electrónica, Puebla, México*

(*Received 18 February 2014; accepted 20 April 2014*)

We investigate the enhancement of characteristic nonlinear phase shift in warm rubidium vapor for a signal beam using an additional pump laser at different frequency. A numerical model based on density matrix formalism is used. Experimental results of self-rotation and diffraction in a three-wave mixing process as well as beam amplification are shown. For $^{87}$Rb transition D2 line with $F_g = 1$, the nonlinearity to absorption ratio can be enhanced approximately two times with a pump beam tuned at $F_g = 2$ transition in a co-propagating scheme, which produces strong nonlinear interaction for $F_g = 1$ line at signal beam powers of ~10 mW.

**Keywords:** rubidium vapor; polarization self-rotation; modulation instability



## 1. Introduction

Rubidium vapor close to the atomic transition is well-known optical nonlinear material [1]. Recently, there is an effort to use the rubidium vapor nonlinearity for applications, in particular for dynamic interferometry and electromagnetic vacuum squeezing [2–6]. The figure of merit for such applications is usually determined by the nonlinearity $\eta$ to absorption $\alpha$ ratio ($R = \eta/\alpha$), which gives a characteristic obtainable nonlinear phase shift; thus maximizing this parameter is of interest.

Often, the nonlinearity in rubidium is described as having a scalar Kerr type, being its strength directly proportional to light intensity and inversely proportional to frequency detuning cube $\Delta^3$. This approximation, resulting from a two-level model, is valid far enough from the absorption lines [1]. The absorption far from the line diminishes as $1/\Delta^2$, thus $R \sim 1/\Delta$ there. It is clear, that if one is interested in obtaining bigger nonlinear phase shifts for moderate intensities, it is necessary to work well inside the lines, where the complete transition structure has to be taken into account for an adequate theoretical description. For these conditions, however, optimal nonlinearity is obtained not for a scalar Kerr interaction, but for more complicated vectorial process, which in general involves elliptic polarizations. Different from Kerr nonlinearity whose strength grows proportional to intensity, in a vectorial case there is an optimal light intensity, and the nonlinearity for intensities higher than the optimal one diminishes. The nonlinearity depends also on flight time of an atom in a beam, and it can be additionally enhanced by a combination of elliptic polarization and weak longitudinal magnetic field [7].

Here, we investigate the possibility to improve the nonlinearity to absorption ratio in D2 Rb line (780 nm) for a signal beam using an independent co- or counter-propagating pump beam tuned at different frequency. We obtained the improvement of ~2 times using additional illumination at resonance with $F_g = 2$ line and for signal at $F_g = 1$ line. In this case, strong amplification in three beam mixing and beam break-up can be observed, which are not obtained in this line without a pump [7]. The numerical modeling compares reasonably with the experimental results.

## 2. Numerical results

A simple nonlinear process, which for moderate light intensities can be more efficient than scalar Kerr nonlinearity, is the polarization self-rotation of elliptically polarized beam induced by cross-phase modulation of two circularly polarized components. The general mechanism of this nonlinearity in rubidium involves an ac-Stark effect [8,9]. A simple $\Lambda$ configuration ($F_g = 1$ to $F_e = 0$) transition, as well as $F_g = 1$ to $F_e = 1$ transition do not demonstrate self-rotation. The reasons for this are explained in detail in [9]. If there exist additional upper levels (for example in double $\Lambda$ configuration [8], or for $F_g = 1$ to $F_e = 2$ transition [9]), the elliptically polarized light separates ground sublevels due to the interaction with an additional level because of ac-Stark effect. This partly breaks the dark state and induces polarization ellipse rotation along propagation. The process efficiency is affected by pumping of additional sublevels, thus it is reasonable to suggest that additional illumination can

*Corresponding author. Email: ymtorresg@inaoep.mx

modify, and in particular enhance nonlinearity by changing level populations.

To calculate the rubidium atom response to the illumination by two laser beams, we model the temporal dynamics of full density matrix for $^{87}$Rb transition Doppler broadened D2 lines with $F_g = 1$ and $F_g = 2$. The details of numerical model are described in our previous papers for the case of a single laser frequency [7,10]. The first principle calculation is based on a specially designed fast algorithm of split step type. The model does not have fitting parameters, and it was shown to give satisfactory description of a number of nonlinear processes for a case of a single laser frequency involved [7]. For two frequencies $\omega_1$ and $\omega_2$, the model modification is quite straightforward, but for validity of rotating wave approximation, we need to assume that both laser frequencies as well as their difference $\omega_1 - \omega_2$ are much bigger than the Rabi frequencies and the characteristic separation between the excited levels. This assumption is justified when one beam is tuned into $F_g = 1$ line, and another in $F_g = 2$ line. In our experiment, we have the signal tuned at $F_g = 1$ transition and the pump at $F_g = 2$.

Without the pump, the maximal self-rotation for a signal beam for $F_g = 1$ is obtained for typical intensities in ~1–10 mW/mm$^2$ range (the value depends on beam diameter). The maximal self-rotation to absorption ratio is obtained for somewhat higher intensities, because the absorption is smaller for higher intensities, but finally the self-rotation diminishing with higher intensities becomes more important, than absorption length growth. We have conducted simulation for the signal beam intensity, which is close to the optimal one (giving the highest $R$), for a signal beam without a pump.

The typical results of simulation are presented in Figures 1 and 2. They were made for intensity levels and characteristic times of flight typical for our

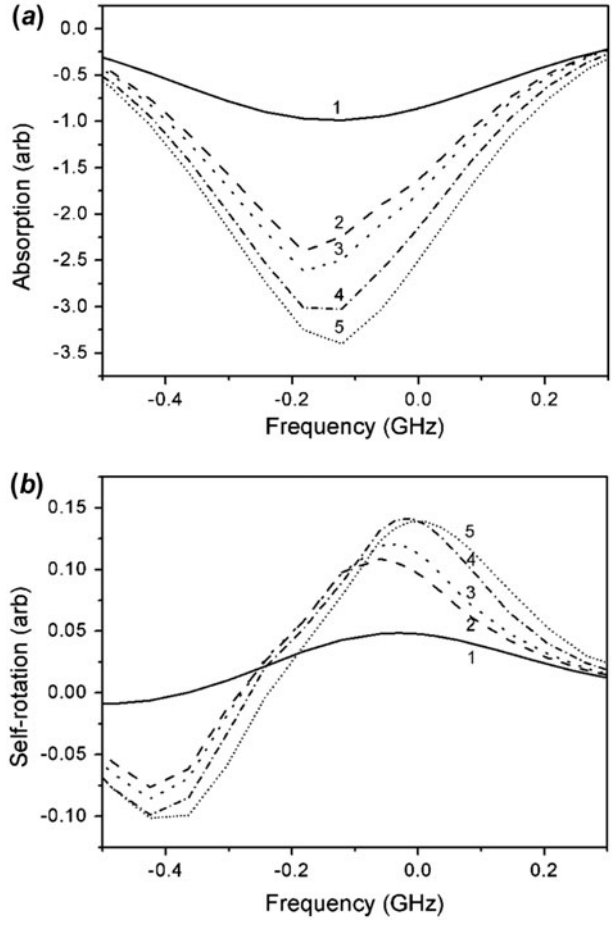


Figure 1. Calculated absorption line shape (*a*) and self-rotation spectrum (*b*) for counter-propagating pump, for signal beam intensity 8.54 mW/mm$^2$ and pump beam intensities: curve 1: 0.0 mW/mm$^2$, curve 2: 12.3 mW/mm$^2$, curve 3: 19.2 mW/mm$^2$, curve 4: 43.2 mW/mm$^2$ and curve 5: 76.9 mW/mm$^2$. The characteristic time of flight is 4.1 μs.

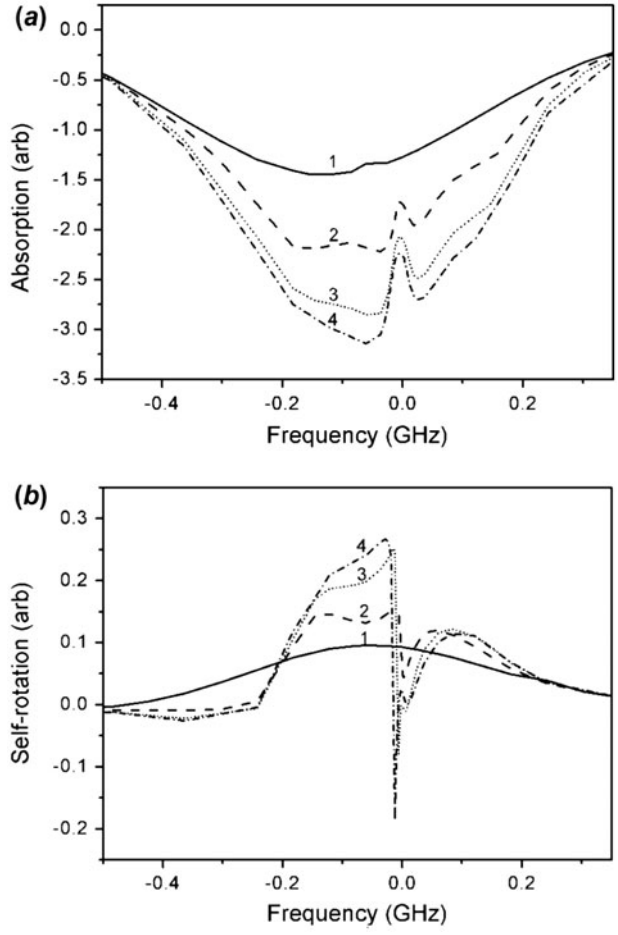


Figure 2. The same, as in Figure 1, but for co-propagating pump. The pump intensities are: curve 1: 0.0 mW/mm$^2$, curve 2: 2.1 mW/mm$^2$, curve 3: 8.54 mW/mm$^2$ and curve 4: 13.3 mW/mm$^2$.

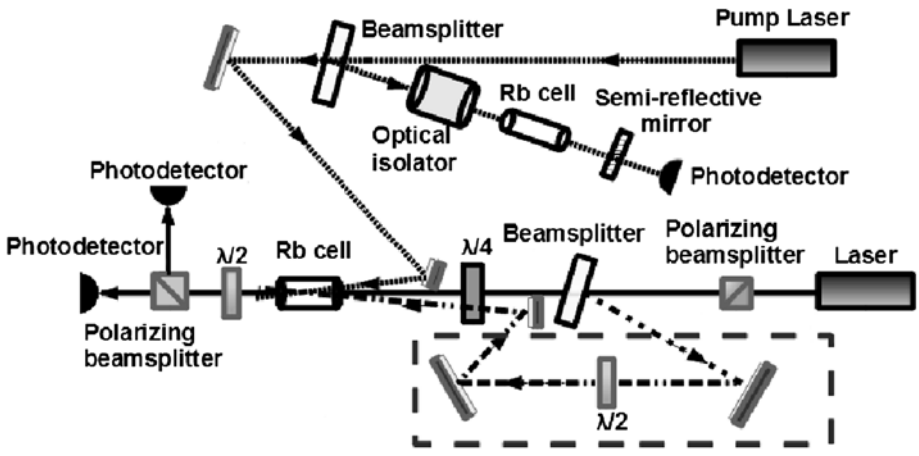


Figure 3. Experimental setup.

experiment. The pump laser frequency was fixed at resonance with $F_g = 2$, $F_e = 2$ transition of an atom at rest, this frequency corresponds to zero detuning in graphs. The calculation results are different for pump beam co- and counter-propagating with respect to a signal one. Physically, the reason for the difference is probably the following. In the case of co-propagating pump and signal beams, the resonant condition that fixes the Doppler-corrected laser frequencies difference can be valid for all atomic velocities. For the counter-propagating case, it can be valid only for a small group of atoms. Thus, coherent effects influence a co-propagating geometry resulting in narrow spectral features which are washed out by an atomic movement in a counter-propagating geometry. It is seen that in any case raising the pump beam intensity makes absorption higher. The absorption growth in presence of pump is easily understood in terms of level populations: the pump transfers

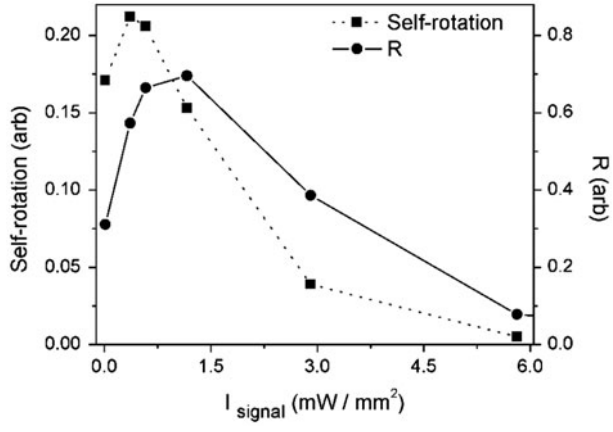


Figure 4. Self-rotation and rotation to absorption ratio $R$ as a function of the signal intensity without the pump beam.

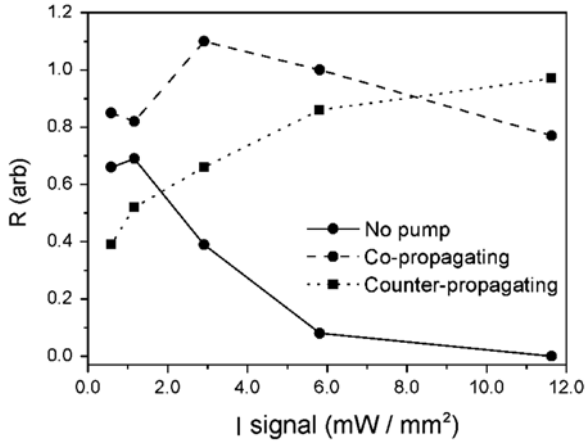


Figure 5. Comparative curves of $R$ as a function of signal intensity without and with the pump beam. Both co- and counter-propagating pump laser cases are shown. The intensity of pump is at maximum (2.22 mW/mm$^2$).

part of the population from $F_g = 2$ level back to $F_g = 1$ level, which is otherwise depleted by a signal.

Though both self-rotation and absorption grow for higher pump intensities, there is an overall growth of $R$, which is obtained for optimal pump intensity, which is of an order of signal intensity. The self-rotation and absorption curves for a signal with a co-propagating pump demonstrate a narrow spectral feature for a frequency corresponding to a pump laser frequency. As mentioned before, for the counter-propagation case this feature is absent. For a co-propagating case, the figure of merit ($R$) is higher in a vicinity of a narrow feature. The calculation shows that the optimal pump intensity exists, and it is lower than for counter-propagating case. The calculation also suggests that co-propagating pump is more efficient, than the counter-propagating, though the enhanced $R$ is observed in both cases.

The calculations for two laser frequencies are very time-consuming because of large number of parameters involved. One can vary the pump frequency and intensities of two beams. There also limitations due to non-uniform intensity profile of both beams. However, the theoretical graphs of Figures 1 and 2 correspond qualitatively to experimental data on self-rotation and three-beam interaction.

## 3. Experimental results

In our experiments, we used two independent tuneable diode external cavity lasers near 780 nm, with 50 mW (signal), and 60 mW (pump). The signal beam inside the cell has an elliptic profile with axes 0.91 mm (horizontal) and 1.21 mm (vertical) (FWHM). The heated rubidium cell 75 mm long was protected with a double μ-metal shield and placed within a solenoid in order to produce a longitudinal magnetic field B. The resistive heater was located between the two shells. Using an additional control cell, the saturated-absorption spectroscopy lines for pump beam are obtained and used for frequency fixing of the pump laser light. A series of three experiments was realized to compare the efficiency of system with and without the pump beam: self-rotation, three-wave mixing and beam amplification with break-up. The basic experimental setup used in all experiments, is shown in Figure 3. An additional weak beam is incorporated for the three-wave mixing and amplification experiments (dashed box in Figure 3).

To observe the effect of pump laser tuned in $^{87}$Rb D2 line, the frequency of the pump beam was fixed and

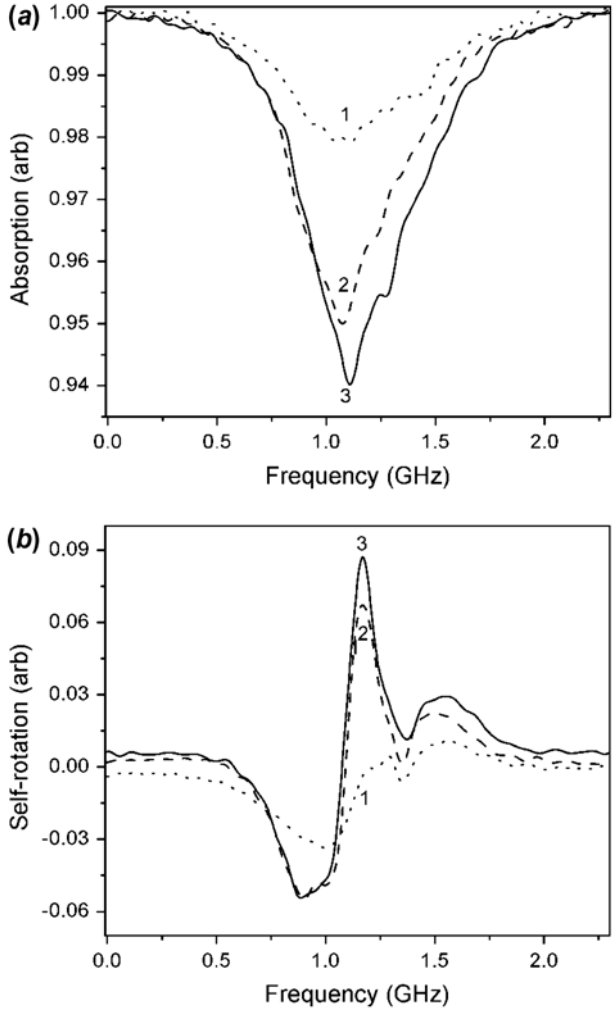


Figure 6. $F_g = 1$ absorption (*a*) and self-rotation (*b*) curves in counter-propagating case when pump beam intensity is: curve 1: 0 mW/mm$^2$, curve 2: 1.11 mW/mm$^2$ and curve 3: 2.22 mW/mm$^2$ and signal intensity is at maximum (11.61 mW/mm$^2$).

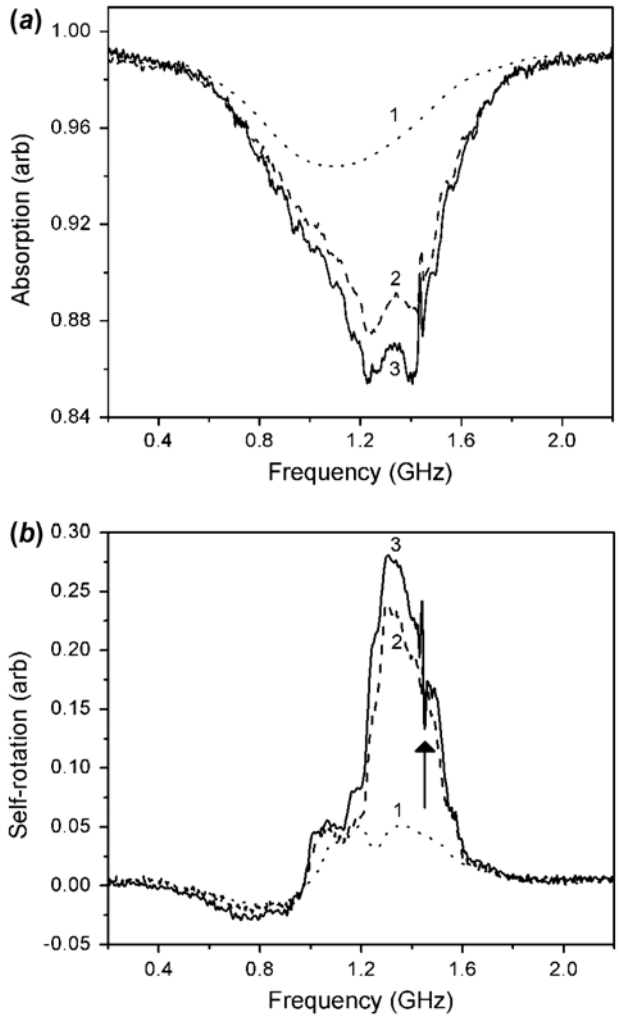


Figure 7. The same, as in Figure 6, but for co-propagating pump with signal intensity 2.9 mW/mm$^2$. The arrow shows the narrow spectral feature corresponding to the pump beam frequency.

the signal laser was scanned across a transition. The pump and the signal beams intersect inside the cell with a small angle (~13 mrad in a vertical plane). Two different types of effects are observed depending on whether both beams are resonant with a same Doppler broadened transition from a ground state, or they act on different transitions. If the pump beam acts on the same $F_g$ transition, as the signal, the absorption for signal beam is diminished, and self-rotation can be enhanced in a part of the line. In the other case, both the absorption and nonlinearity for the signal beam are enhanced. The self-rotation experiments were performed when the pump beam acts on the transitions $F_g = 1$ and $F_g = 2$ and the signal beam on $F_g = 1$. The $R$ ratio can be enhanced in both cases. In this article, we show only the case when the pump frequency is fixed at $F_g = 2$, $F_e = 2$ transition, where somewhat bigger enhancement of rotation to absorption ratio was found and a theoretical model was developed.

### 3.1. *Self-rotation*

The experimental setup for self-rotation measurement is quite standard (see e.g. Rochester et al. [9] and Ries et al. [11]). The first polarizing beamsplitter cube gives a well defined initial vertical polarization in the signal beam. A quarter-wave plate produces a beam with controlled elliptic polarization (±4° plate rotation angle).

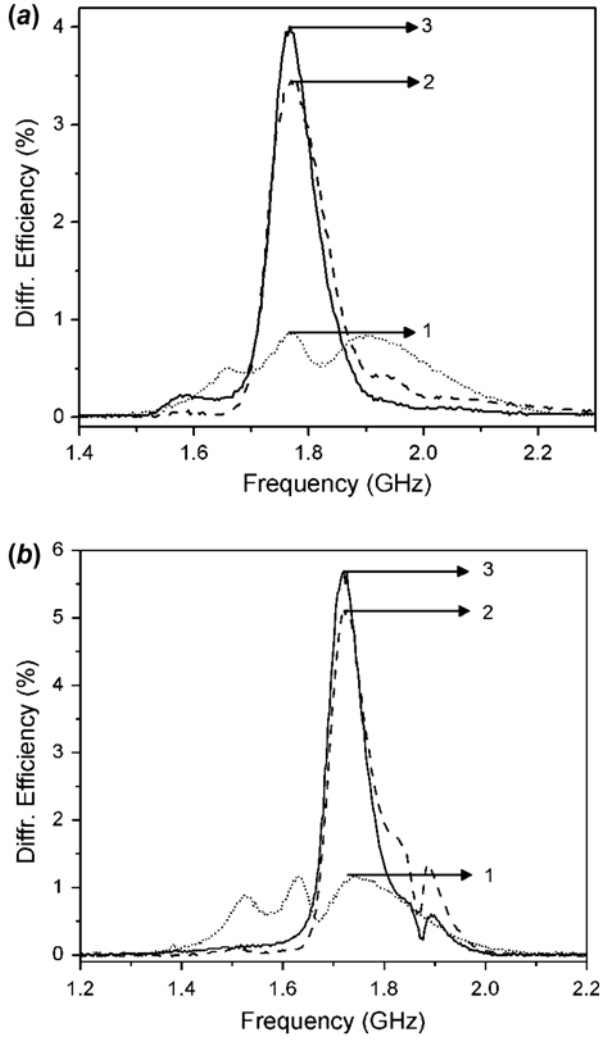


Figure 8. Diffraction efficiency in a conjugated beam: curve 1: Without pump beam, curve 2: With pump beam and curve 3: With pump, $B$ and $e$. The signal intensity is 2.9 mW/mm$^2$ and pump beam intensity is at maximum (2.22 mW/mm$^2$). (*a*) Counter-propagating case with $B = 0.455$ mT and $e = 10°$. (*b*) Co-propagating case with $B = 0.331$ mT and $e = 10°$.

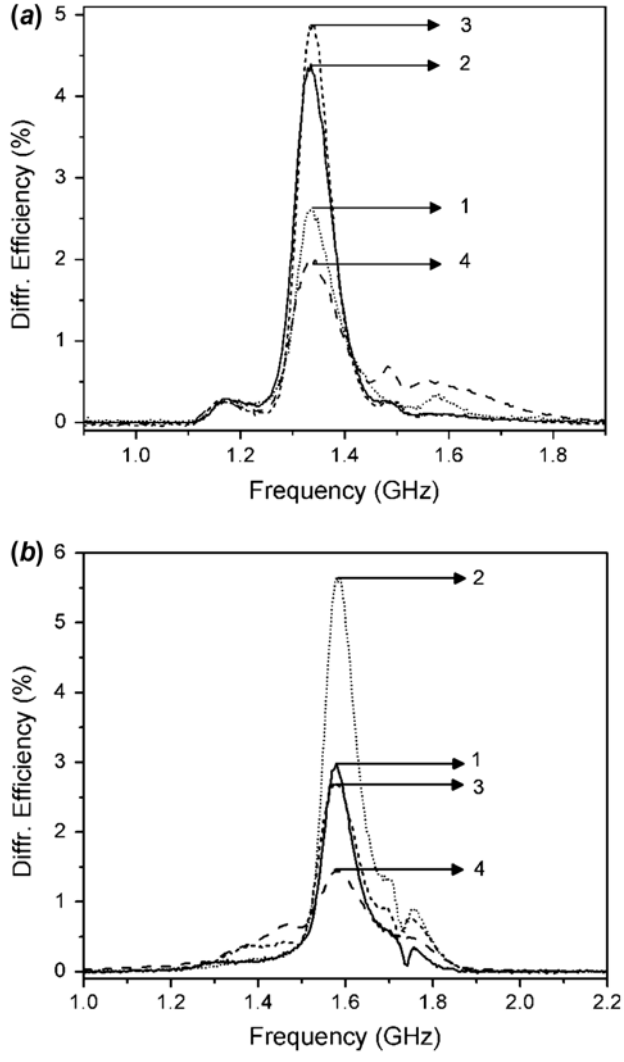


Figure 9. Diffraction efficiency in a conjugated beam when signal intensity is changed: Curve 1: 1.16 mW/mm$^2$, curve 2: 2.9 mW/mm$^2$, curve 3: 5.8 mW/mm$^2$ and curve 4: 11.61 mW/mm$^2$. The pump beam intensity is 2.22 mW/mm$^2$. (*a*) Counter-propagating and (*b*) co-propagating case. The values of $B$ and $e$ are the same that in Figure 8.

The output half-wave plate is followed by a polarizing beamsplitter and a differential photodetector. The signal beam is frequency scanned, and the half-wave plate is rotated until signals for two photodetectors are equal far from the absorption line. The difference signal from photodetector pair is proportional to polarization ellipse rotation angle [9]. The sum of these two signals gives a measure of absorption. In the experimental setup scheme (Figure 3), the pump beam is shown in the co-propagating configuration, but the experiments were also performed impinging the pump beam in a counter-propagating direction.

The absorption and rotation values (and therefore $R$) depend on the signal and pump beam intensities. The dependence of self-rotation and $R$ on signal intensity without the pump beam is in a good agreement with theoretical description of Section 2. The Figure 4 shows that the self-rotation reaches the maximal value when the signal is 0.36 mW/mm$^2$, but $R$ is maximal when this value is 1.16 mW/mm$^2$. In Figure 5 the comparative curves of $R$ as a function of signal beam intensity with and without the pump are shown. The value of $R$ is maximal for the co-propagating case when signal intensity is 2.9 mW/mm$^2$.

We also checked the dependence of $R$ on the pump beam intensity (fixing the signal to optimal intensity according to Figure 5) and found that the higher is the pump beam intensity, the higher is the value of $R$ for our experimental signal to pump intensity ratio (~5). Figures 6 and 7 show absorption and self-rotation curves when the pump is absent and for two different values of pump intensity. The value of $R$ is enhanced when the pump beam is present for both co- and counter-propagating cases, but better increment (~2 times related to case without the pump beam) was obtained in the first case. The narrow spectral feature in curves for the co-propagating case can be seen in Figure 7.

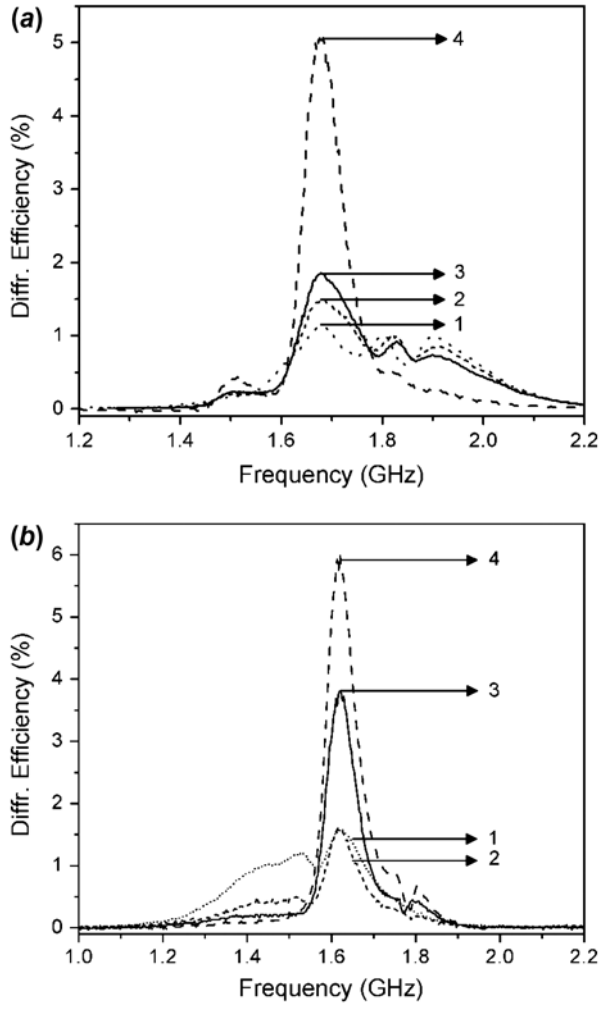


Figure 10. Diffraction efficiency in a conjugated beam with different pump intensity values: curve 1: 0.28 mW/mm$^2$, curve 2: 0.55 mW/mm$^2$, curve 3: 1.11 mW/mm$^2$ and curve 4: 2.22 mW/mm$^2$. (*a*) Counter-propagating pump with signal intensity 5.8 mW/mm$^2$ and (*b*) co-propagating pump with signal intensity 2.9 mW/mm$^2$. The values of $B$ and $e$ are the same that in Figure 8.

### 3.2. *Three-wave mixing*

For a second series of experiments, a weak additional beam is incorporated in the experimental setup (dotted box in Figure 3), in a form similar to that of Refs. [12,13]. The weak beam has an intensity of 4% of signal beam and passes through a half-waveplate in order to obtain an initial polarization perpendicular to that one of the signal beam. The diffraction in a conjugated order

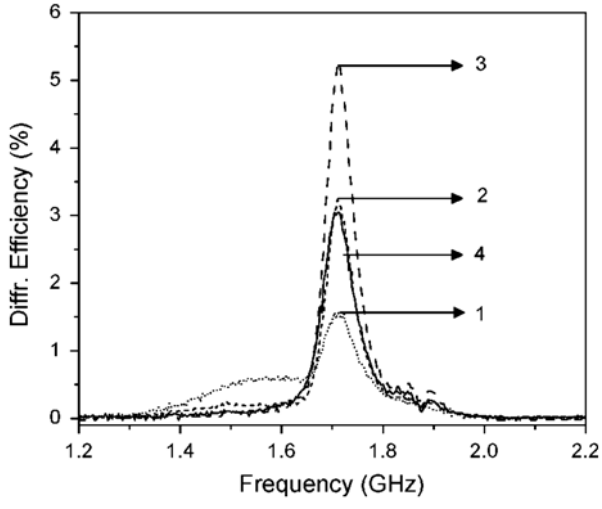


Figure 11. Diffraction efficiency for co-propagating case when signal intensity is 1.16 mW/mm$^2$. The values of pump intensity are the same that in Figure 10.

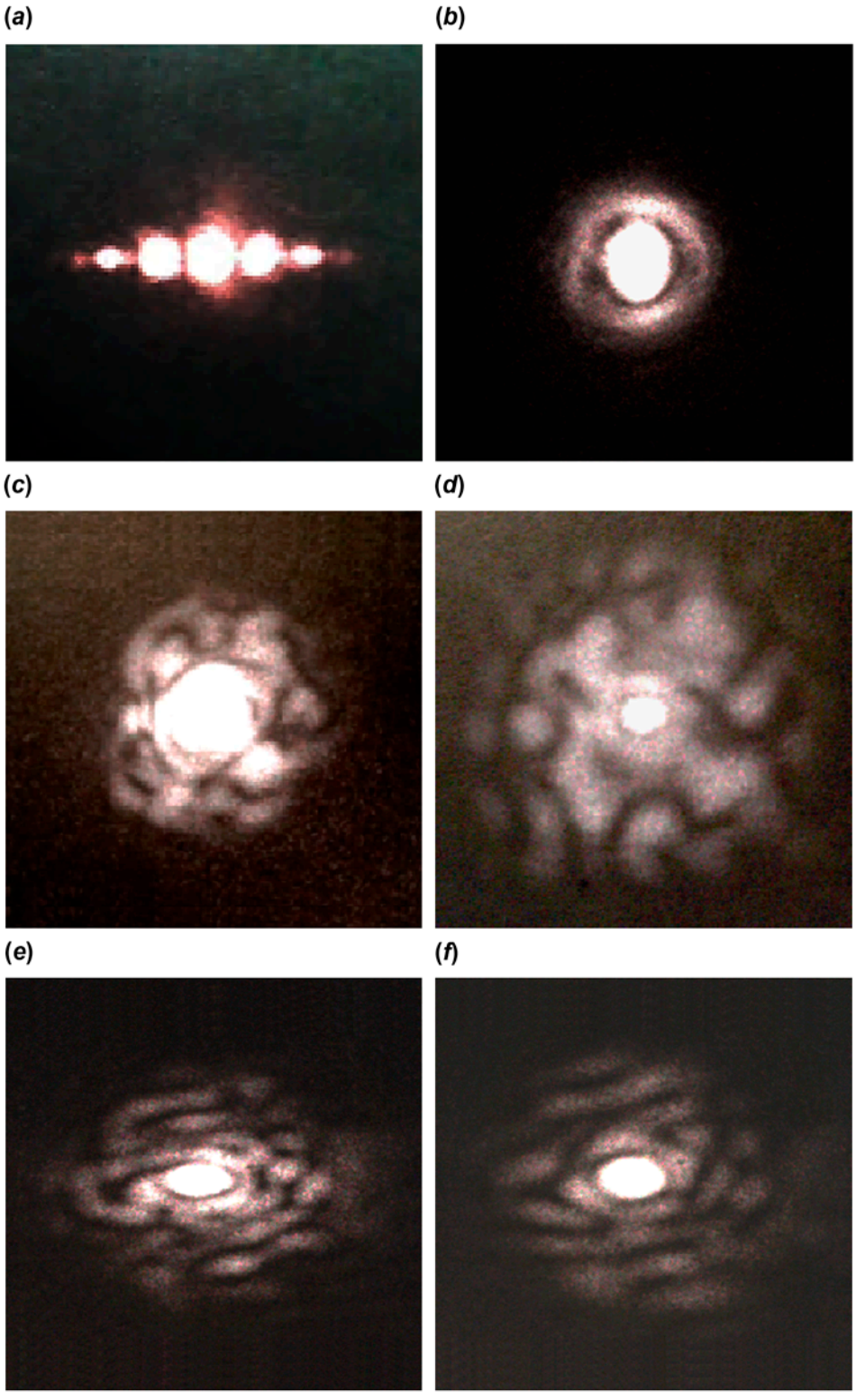


Figure 12. Patterns generated in the far field for co- and counter-propagating schemes: (*a*) Diffraction orders in counter-propagating case with $T = 117\,^{\circ}\mathrm{C}$, $e = 3.5^{\circ}$, $B = 0.333$ mT. (*b*) The ring in co-propagating case with $T = 125\,^{\circ}\mathrm{C}$, $e = 10^{\circ}$ and $B = 0.223$ mT. Counter-propagating breakup patterns with $B = 0.306$ mT and $e = 3.5^{\circ}$: (*c*) $T = 119\,^{\circ}\mathrm{C}$, (*d*) $T = 122\,^{\circ}\mathrm{C}$. Co-propagating breakup patterns with $B = 0.223$ mT, $e = 10^{\circ}$: (*e*) $T = 134\,^{\circ}\mathrm{C}$, (*f*) $T = 141\,^{\circ}\mathrm{C}$. (The colour version of this figure is included in the online version of the journal.)

was observed for cell temperature 80 °C. The half-wave-plate, polarizing beamsplitter and differential photodetector at the end of the cell are replaced in this case by a single photodetector where the conjugated order was detected. The diffraction efficiency depends strongly on the parameters of the system such as the angle between signal and pump laser, the angle between signal and weak beam (4 mrad), the pump and signal intensities, polarization ellipticity and magnetic field.

In order to find the parameters to obtain the optimal diffraction efficiency, the intensity of signal and pump beams were fixed and the diffraction without and with pump beam was measured. Additionally, when the pump is present, a weak longitudinal magnetic field B (<0.5 mT) and polarization ellipticity were applied to increase the diffraction curve maximum. The temperature is selected in each case to obtain the same absorption of 50%. The Figure 8 shows the diffraction efficiency for the three cases described before with the pump beam intensity maximal and the signal beam intensity at 2.9 $mW/mm^2$. The better value of diffraction efficiency is obtained with the pump beam and it is increased slightly when $B$ and $e$ are present in both cases (co- and counter-propagating). As might be expected from Figure 5, the efficiency is higher for the co-propagating case.

The dependence of diffraction efficiency on signal (Figure 9) and pump (Figure 10) intensities was studied. In Figure 9, where pump beam, $B$ and $e$ are present, the values of the optimal signal intensity in co- and counter-propagating cases are different. In Figure 10 it is seen, that the maximal diffraction efficiency is obtained for maximal pump beam intensity. However, the existence of a saturation pump intensity can be verified if the signal beam intensity is fixed to less of 1.16 $mW/mm^2$, so that the ratio signal/pump is diminished enough to obtain saturation as is shown in Figure 11 for the co-propagating case.

### 3.3. *Beam amplification and breakup*

In the last experiment, patterns were generated in the far field due to a strong exponential amplification in a three-wave mixing process related to modulation instability mechanism [1,7]. The patterns were observed in co- and counter-propagating schemes and for different values of signal intensity, magnetic field and polarization ellipticity. The additional weak beam incorporated in our previous experiment was made even weaker. The first observed pattern at $T = 80$ °C corresponds to the conjugated order. By raising temperature ($T = 117$ °C or more), it is possible to see formation of higher orders of diffraction for an appropriate geometry (Figure 12(*a*)). When additional beam is much weaker than a signal (1000 times), and the temperature is high (>120 °C), different types of patterns surrounding signal beam can be observed starting with a ring (Figure 12(*b*)), passing through a transition pattern (Figure 12(*c*)) and (*e*)) and ending with a breakup of beam (Figure 12(*d*) and (*f*)). The patterns in Figure 12(*a*) and (*b*)) are similar for co- and counter-propagating schemes, and with higher temperatures the pattern is highly sensitive to changes in the parameters $B$, $e$, signal intensity and beams geometry. In the co-propagating case, as well as in the counter-propagating, it is possible to reach amplifications of more than 100 times.

The influence of the magnetic field on the nonlinear coefficients without an additional pump was discussed in Ref. [7]. Although a combination of longitudinal magnetic field and polarization ellipticity in the three-wave mixing experiments can increase slightly the value of diffraction efficiency, the experiment shows that the main contribution is obtained here with a pump beam alone. Because of this, we have limited our simulation to zero magnetic field. For high amplifications related to developed modulation instability, even slight changes in parameters such as laser frequencies, polarization, beam geometry and magnetic field give rise to pronounced changes in a pattern, but the pattern itself tends to develop as speckle, and not as a small number of well-separated spots, characteristic for experiments with feedback (e.g in resonators).

## 4. Discussion and conclusions

In conclusion, we show that using an additional illumination with a pump beam tuned at $F_g = 2$ line, the polarization self-rotation, rotation to absorption ratio and diffraction efficiency in $^{87}$Rb D2 line can be enhanced for a signal beam tuned into $F_g = 1$ line. The effect is reproduced in a numerical calculation for full density matrix evolution and the results show a reasonable qualitative agreement with experimental results. A gain in nonlinearity to absorption ratio of ~2 times for a co-propagating scheme was achieved, which allows strong beam amplification (>100 times) in three-wave mixing, and break-up effects, which are not observed in this line without additional illumination. The results suggest that this mechanism can possibly be useful for enhancing efficiency in squeezing experiments.

## Acknowledgment

This research was partly performed in the framework of Consejo Nacional de Ciencia y Tecnología project 156891.

## References

[1] Zerom, P.; Boyd, R.W. In *Self-focusing, Past and Present, Topics in Applied Physics*, Vol. 114; Boyd, R.W., Lukishova, S.G., Shen, Y.R., Eds.; Springer Science + Business Media: New York, 2009; Chapter 9; pp. 231–251.

[2] Matsko, A.B.; Novikova, I.; Welch, G.R.; Budker, D.; Kimball, D.F.; Rochester, S.M. *Phys. Rev. A* **2002,** *66*, 043815-1–043815-10.
[3] Mikhailov, E.E.; Lezama, A.; Noel, T.W.; Novikova, I. *J. Mod. Opt.* **2009,** *56*, 1985–1992.
[4] Agha, I.H.; Messin, G.; Grangier, P. *Opt. Exp.* **2010,** *18*, 4198–4205.
[5] Liu, C.; Jing, J.; Zhou, Z.; Pooser, R.C.; Hudelist, F.; Zhou, L.; Zhang, W. *Opt. Lett.* **2011,** *36*, 2979–2981.
[6] Horrom, T.; Romanov, G.; Novikova, I.; Mikhailov, E. *J. Mod. Opt.* **2013,** *60*, 43–49.
[7] Korneev, N., Gutiérrez Parra, C. *J. Opt. Soc. Am. B* **2012,** *29*, 2588–2594.
[8] Novikova, I.; Matsko, A.B.; Welch, G.R. *J. Mod. Opt.* **2002,** *49*, 2565–2581.
[9] Rochester, S.M.; Hsiung, D.S.; Budker, D.; Chiao, R.Y.; Kimball, D.F.; Yashchuk, V.V. *Phys. Rev. A* **2001,** *63*, 043814-1–043814-10.
[10] Korneev, N.; Benavides, O. *J. Mod. Opt.* **2009,** *56*, 1194–1198.
[11] Ries, J.; Brezger, B.; Lvovsky, A.I. *Phys. Rev. A* **2003,** *68*, 025801-1–025801-4.
[12] Korneev, N.; Soto, J. *Opt. Commun.* **2005,** *245*, 437–442.
[13] Korneev, N.; Benavides, O. *J. Opt. Soc. Am. B* **2008,** *25*, 1899–1906.